



Cite this: *Nanoscale Adv.*, 2023, **5**, 3985

A polyoxometalate-based heterojunction nanozyme with peroxidase-mimic catalytic activity for sensitive biomolecule detection

Guobo Du, ^{ab} Mingzhu Lv, ^{cd} Huan Wang, ^{cd} Chenghui Liu, ^{cd} Qiqi Xu, ^{cd} Jiajie Liu, ^{cd} Zhu Yang, ^{cd} Yuan Yong ^{*cde} and Yunwei Han ^{*af}

Nanozymes are a class of nanomaterials that can specifically mimic the structures and catalytic activities as well as overcome limitations of natural enzymes and have hence been considered as a competitive alternative to natural enzymes. At present, plenty of nanozymes, especially those with peroxidase (POD)-like catalytic activity, have been extensively explored for biosensing. In this work, we proposed polyoxometalate-based heterojunction $\text{GdP}_5\text{W}_{30}\text{O}_{110}@\text{WS}_2$ nanoclusters (NCs) to exert intrinsic POD-like catalytic activity even under harsh catalytic conditions. Detailedly, $\text{GdP}_5\text{W}_{30}\text{O}_{110}@\text{WS}_2$ NCs possessing conducive POD-like catalytic activity can oxidize chromogenic substrates into colored substances in the presence of H_2O_2 . On the strength of the POD-like catalytic activity of $\text{GdP}_5\text{W}_{30}\text{O}_{110}@\text{WS}_2$ NCs, a reliable analytical platform is then constructed after the optimization of catalytic conditions for the detection of H_2O_2 , glutathione (GSH) and glucose via a simple TMB colorimetric strategy. This work advances the utilization of versatile polyoxometalate-based nanomaterials for biosensing, dramatically broadening the potential applications of other nanozyme-based biosensors.

Received 2nd April 2023

Accepted 15th June 2023

DOI: 10.1039/d3na00210a

rsc.li/nanoscale-advances

Introduction

Biomolecules play crucial roles in diverse physiological and pathological processes, and their levels in the human body can serve as important indicators for monitoring physical status.^{1,2} Therefore, highly selective and sensitive quantitative detection of biomolecules not only helps to reveal their functions in various physiological processes but also is a prerequisite and basis for monitoring the physical status of the human body.^{3,4} Of note, benefiting from the specificity of active enzymes to substrates, enzymatic methods can achieve rapid and accurate biomolecule detection, which is one of the most mature and

commonly applied typical strategies.^{5,6} Natural enzymes are a class of proteins possessing high substrate specificity and efficacious catalytic activity and are implicated in almost all biocatalytic reactions in organisms.^{7,8} However, their practical applications are severely limited by intrinsic shortcomings such as high cost, susceptibility to environmental factors, and difficult purification.^{9,10} To overcome these drawbacks, it is of great importance to develop novel artificial enzyme mimics that have remarkable enzyme-like activities by facile synthesis. Since the first demonstration of the peroxidase (POD)-like property of Fe_3O_4 nanoparticles by Gao in 2007, many nanomaterials with multiple enzymatic catalytic activities, namely nanozymes, have been considered as strong substitutes for nature enzymes and have been widely used in biological, medical and industrial catalysis fields.¹¹ So far, a surge of artificial nanozymes with POD-like catalytic activity, such as precious metals, metal oxides, transition metal dichalcogenides (TMDs), carbon-based nanomaterials, single-atom nanozymes and metal-organic frameworks (MOFs), have been extensively utilized for biosensing.¹²⁻¹⁸ However, their enzymatic catalytic efficiency is still far less than that of natural enzymes. Thus, investigations on nanozymes with efficient catalytic activity, minimal cytotoxicity and high affinity to substrates are still imperative and pivotal.

In recent years, emerging kinds of metal-based nanomaterials with shifting or mixed redox states have been found to exert intrinsic POD-like catalytic activity.^{19,20} However, the insufficient enzymatic performance of these nanomaterials is

^aJinan University, No. 601, Huangpu Avenue West, Guangzhou 510630, China. E-mail: yongy1816@163.com; 530018842@qq.com

^bDepartment of Oncology, Affiliated Hospital of North Sichuan Medical College, No. 1 Maoyuan South Road, Shunqing District, Nanchong, Sichuan 637000, China

^cKey Laboratory of Pollution Control Chemistry and Environmental Functional Materials for Qinghai-Tibet Plateau of the National Ethnic Affairs Commission, School of Chemistry and Environment, Southwest Minzu University, Chengdu 610041, China

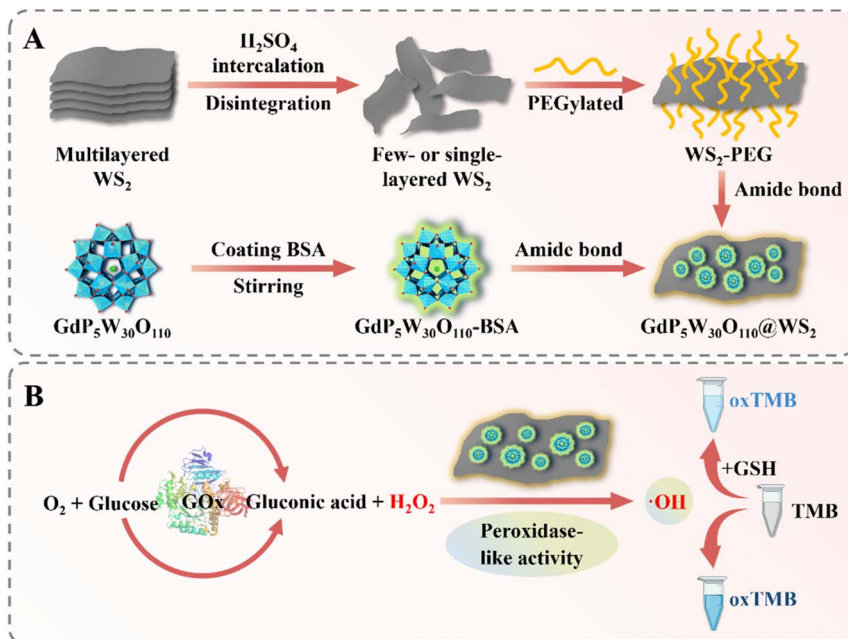
^dKey Laboratory of General Chemistry of the National Ethnic Affairs Commission, School of Chemistry and Environment, Southwest Minzu University, Chengdu 610041, China

^eCentral Nervous System Drug Key Laboratory of Sichuan Province, School of Chemistry and Environment, Southwest Minzu University, Chengdu 610041, China

^fDepartment of Oncology, The Affiliated Hospital of Southwest Medical University, Luzhou, 646000, Sichuan, China

[†] These authors contributed equally.





Scheme 1 (A) Schematic illustration of the general synthetic procedures of the $\text{GdP}_5\text{W}_{30}\text{O}_{110}\text{@WS}_2$ nanozymes; (B) Mechanism description of $\text{GdP}_5\text{W}_{30}\text{O}_{110}\text{@WS}_2$ nanozymes with peroxidase-like activity for the colorimetric detection of biomolecules, including H_2O_2 , GSH and glucose.

inadequate for their applications in the fields of biosensing. Since most of the reactions take place on the surface of nanozymes, we speculate that surface modification or increasing the specific surface area of nanozymes enables higher catalytic activity for a more sensitive enzymatic reaction.²¹ Interestingly, constructing a heterojunction structure can also further enhance the enzymatic activity of these nanozymes *via* accelerating the electron transfer on the heterogeneous interface and reducing the required energy for the binding between nanozymes and H_2O_2 .^{22–24} Based on the aforementioned findings, we assume that polyoxometalate-based heterojunctions can act as prospective POD-like nanozymes for biosensing.

Herein, polyoxometalate-based heterostructure $\text{GdP}_5\text{W}_{30}\text{O}_{110}\text{@WS}_2$ NCs were constructed (Scheme 1A). Benefiting from the specific heterostructure and high specific surface area inherited from WS_2 nanosheets, the prepared $\text{GdP}_5\text{W}_{30}\text{O}_{110}\text{@WS}_2$ exhibited a remarkable POD-like catalytic performance and superior tolerance to stringent conditions. Furthermore, $\text{GdP}_5\text{W}_{30}\text{O}_{110}\text{@WS}_2$ was implicated in a facile colorimetric platform to realize the quantitative detection of H_2O_2 , glutathione (GSH) and glucose. The excellent analytical performance manifested that our work opens up broad prospects for the elaborate design and development of polyoxometalate-based nanozymes and dramatically expands the potential application of nanzyme-based biosensors.

Experimental section

Chemicals

Sodium tungstate dihydrate ($\text{Na}_2\text{WO}_4 \cdot 2\text{H}_2\text{O}$), bovine serum albumin (BSA), 1-(3-dimethylaminopropyl)-3-ethylcarbodiimide (EDC) and *N*-hydroxysuccinimide (NHS) were obtained from

Aladdin Industrial Corporation (Shanghai, China). Gadolinium(III) chloride hexahydrate ($\text{GdCl}_3 \cdot 6\text{H}_2\text{O}$) and tungsten sulfide (WS_2 , 99.8%) were purchased from Alfa Aesar Reagent Company (Shanghai, China). Sodium acetate (NaAc), acetic acid (HAc), citric acid monohydrate, disodium hydrogen phosphate anhydrous (Na_2HPO_4), methanol (CH_3OH , 99.5%) and sulfuric acid (H_2SO_4 , 95–98%) were bought from Chron Chemicals Co., Ltd (Shanghai, China). Polyethylene glycol 400 (PEG-400) was supplied by Kermel (Tianjin, China). Ethanol, hydrogen peroxide (H_2O_2 , 30%) and phosphoric acid (H_3PO_4 , 85%) were purchased from Jinshan Chemical Reagent Co., Ltd (Chengdu, China). Potassium acetate (CH_3COOK) and potassium chloride (KCl) were from Tianjin Zhiyuan Chemical Reagent Co., Ltd (Tianjin, China). 3,3',5,5'-Tetramethylbenzidine (TMB) was obtained from Adamas Reagent Co., Ltd. Acetic acid buffer (HAc-NaAc, 0.2 M) and Na_2HPO_4 -citric acid buffer (0.2 M) solutions were prepared in the laboratory. All reagents and solvents were of commercially analytical grade and used as received without any previous purification.

Preparation of $\text{GdP}_5\text{W}_{30}\text{O}_{110}$ nanoclusters

The $\text{GdP}_5\text{W}_{30}\text{O}_{110}$ nanoclusters were synthesized by a two-step hydrothermal approach according to a previously reported procedure with an adjusted dose.²⁵ In a typical synthetic procedure, 16.5 g $\text{Na}_2\text{WO}_4 \cdot 2\text{H}_2\text{O}$ was first completely dissolved in 15 mL ultrapure water with ultrasound assistance and then 85% H_3PO_4 (13.25 mL) was slowly added into the solution. Afterwards, the above mixture was placed into a sample preparation bomb and was heated up to 120 °C for 12 h. After the bomb was spontaneously cooled down to room temperature, ultrapure water (7.5 mL) and KCl (5 g) were added into the



reaction system and some white precipitate was immediately formed. Then, the precipitate was filtered and washed with potassium acetate solution (2 M) and methanol. When the precipitate naturally dried, it was dissolved in 15 mL hot ultrapure water (around 65 °C) and the intermediate product $K_{12.5}Na_{1.5}[NaP_5W_{30}O_{110}] \cdot 15H_2O$ was subsequently formed by cooling and recrystallization.

Then, $K_{12.5}Na_{1.5}[NaP_5W_{30}O_{110}] \cdot 15H_2O$ (1 g) was dissolved in 12 mL ultrapure water and heated to 65 °C. Afterwards, $GdCl_3 \cdot 6H_2O$ aqueous solution (0.08 mmol mL^{-1} , 3 mL) was dropwise added into the above solution under heating with magnetic stirring. After reaction, the mixture was poured into a sample preparation bomb and heated at 160 °C for 12 h. After the bomb was spontaneously cooled down to room temperature, KCl (4 g) was introduced into the reaction system and the precipitate was immediately formed. Then, the precipitate was filtered and washed with potassium acetate solution (2 M) and methanol. Finally, the as-synthesized $GdP_5W_{30}O_{110}$ nanoclusters were air-dried and ready for use.

Surface functionalization of $GdP_5W_{30}O_{110}$ nanoclusters with BSA

In brief, 400 mg BSA and 0.118 g $GdP_5W_{30}O_{110}$ nanoclusters were dispersed into 20 mL ultrapure water and the mixture was stirred for 6 h. The carboxy-functionalized $GdP_5W_{30}O_{110}$ nanoclusters ($GdP_5W_{30}O_{110}$ -BSA) were kept at room temperature for later use.

Preparation of WS_2 nanosheets

The WS_2 nanosheets were synthesized by ultrasound-assisted liquid exfoliation using H_2SO_4 as an intercalation agent by referring to a previous report.²⁶ First, commercial WS_2 powder was ground in a ball miller for 6 h. Next, the preconditioned WS_2 (60 mg) was dispersed into 60 mL concentrated sulfuric acid (H_2SO_4 , 95–98%) and the reaction mixture was kept at 90 °C in an oil bath for 24 h under stirring. Afterwards, the H_2SO_4 -intercalated WS_2 was centrifugally collected at 6000 rpm (10 min) and washed with ultrapure water to remove supernatant H_2SO_4 , repeating four times. Then, the purified H_2SO_4 -intercalated WS_2 was re-dispersed into ultrapure water (about 30 mL) and was ultrasonically peeled off in an ice-cold water bath for 2 h. Finally, the layered WS_2 nanosheets were harvested by centrifugation (12 000 rpm, 20 min).

Surface functionalization of WS_2 nanosheets with PEG-400

To synthesize amino-functionalized WS_2 nanosheets, PEG-400 ethanol solution (50 mg mL^{-1} , 1 mL) was added into layered WS_2 solution (1 mg mL^{-1} , 10 mL), and the mixture was stirred for 12 h at room temperature. Then, the WS_2 -PEG was obtained by centrifugation (6000 rpm, 10 min) and washed with ultrapure water to remove residual PEG-400.

Preparation of $GdP_5W_{30}O_{110}$ @ WS_2

In a typical preparation process, 5 mg 1-(3-dimethylaminopropyl)-3-ethylcarbodiimide (EDC) was first introduced into WS_2 -PEG

aqueous solution (1 mg mL^{-1} , 10 mL) and some white floccules formed immediately. Then, 5 mg *N*-hydroxysuccinimide (NHS) was added and the mixture was set under magnetic stirring until the white floccules disappeared. Afterwards, $GdP_5W_{30}O_{110}$ -BSA (2 mL) was added into the above solution, followed by stirring at room temperature for 12 h. Finally, the as-prepared $GdP_5W_{30}O_{110}$ @ WS_2 was collected by centrifugation (6000 rpm, 10 min) and washed with ultrapure water.

Peroxidase-like catalytic activity of $GdP_5W_{30}O_{110}$ @ WS_2

Peroxidase-like catalytic activity assay. The representative colorimetric analysis assay using 3,3',5,5'-tetramethylbenzidine (TMB), 2,2'-azino-bis(3-ethylbenzothiazoline-6-sulfonic acid) (ABTS), and *o*-phenylenediamine (OPD) as peroxidase colorimetric substrates in the presence of H_2O_2 was performed to preliminarily evaluate the peroxidase-like catalytic activity of $GdP_5W_{30}O_{110}$ @ WS_2 . The hydroxyl radical ('OH) that was generated by a Fenton-like reaction between H_2O_2 and W^{5+} of $GdP_5W_{30}O_{110}$ @ WS_2 can oxidize colorimetric substrates into colored substances with their respective characteristic peaks. Therefore, the peroxidase-like catalytic activity of $GdP_5W_{30}O_{110}$ @ WS_2 can be readily determined *via* monitoring the absorption intensity at characteristic peaks of the reaction system. In general, $GdP_5W_{30}O_{110}$ @ WS_2 (final concentration 100 $\mu g mL^{-1}$) and colorimetric substrates (TMB, ABTS or OPD, final concentration 0.5 mM) were first added into Na_2HPO_4 -citric acid buffer (0.2 M). Subsequently, H_2O_2 (final concentration 50 mM) was introduced into the reacting system to launch the chromogenic reaction. After 30 min incubation, the supernatant was collected by centrifugation (6000 rpm, 10 min) and the absorbance spectrum was recorded with UV-vis spectroscopy (UV-6100, MAPADA).

H_2O_2 and GSH detection by $GdP_5W_{30}O_{110}$ @ WS_2

Briefly, $GdP_5W_{30}O_{110}$ @ WS_2 (final concentration 100 $\mu g mL^{-1}$), TMB ethanol solution (final concentration 0.5 mM) as well as varied concentrations of H_2O_2 (0–50 mM) or different concentrations of GSH (0–25 μM) with 50 mM H_2O_2 were mixed into Hac-NaAc buffer (0.2 M, pH 3.0) and the solution was incubated for 30 min at 50 °C in the dark. Finally, the UV-vis spectrum was recorded by UV-vis spectroscopy.

Glucose detection by $GdP_5W_{30}O_{110}$ @ WS_2

In detail, GOx (final concentration 1 mg mL^{-1}) and various concentrations of glucose aqueous solution (0–1.0 mM) were first mixed together and incubated at 37 °C for 1 h. Afterwards, $GdP_5W_{30}O_{110}$ @ WS_2 (final concentration 100 $\mu g mL^{-1}$) and TMB ethanol solution (final concentration 0.5 mM) were then introduced and the UV-vis spectrum was recorded after 30 min reaction at 50 °C.

Results and discussion

Preparation and characterization of $GdP_5W_{30}O_{110}$ @ WS_2

The concise fabrication process of the heterostructure $GdP_5W_{30}O_{110}$ @ WS_2 NCs is illustrated in Scheme 1A. Here, the easy-



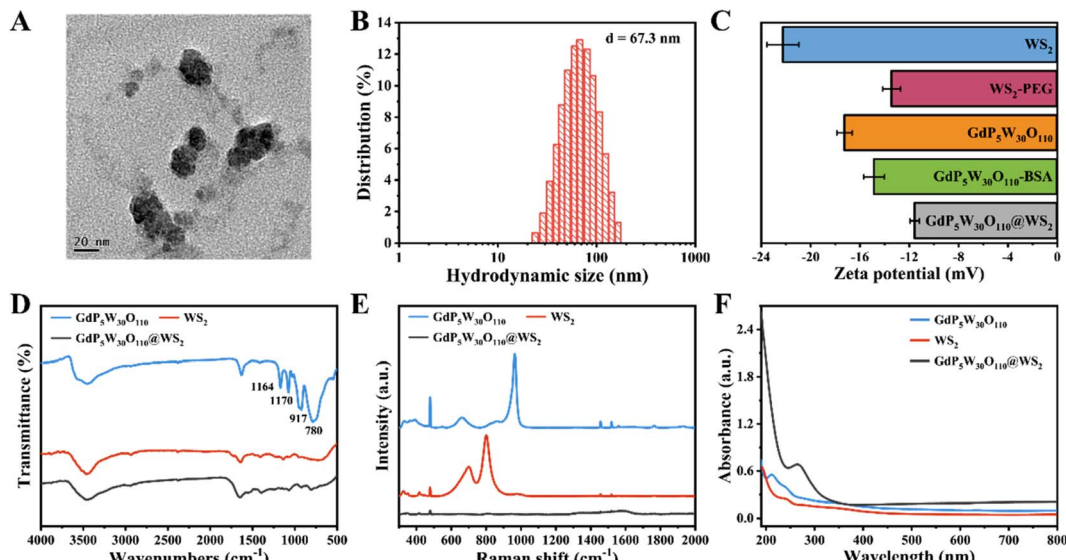


Fig. 1 Preparation and characterization of $\text{GdP}_5\text{W}_{30}\text{O}_{110}@\text{WS}_2$ nanoclusters. (A) TEM image of $\text{GdP}_5\text{W}_{30}\text{O}_{110}@\text{WS}_2$ nanoclusters. (B) Hydrodynamic size distribution of $\text{GdP}_5\text{W}_{30}\text{O}_{110}@\text{WS}_2$ nanoclusters measured by dynamic light scattering (DLS). (C) Zeta potential of $\text{GdP}_5\text{W}_{30}\text{O}_{110}@\text{WS}_2$ and its components. (D) FT-IR spectra and (E) Raman spectra of $\text{GdP}_5\text{W}_{30}\text{O}_{110}$, WS_2 and $\text{GdP}_5\text{W}_{30}\text{O}_{110}@\text{WS}_2$ nanoclusters. (F) UV-vis-NIR adsorption spectra of $\text{GdP}_5\text{W}_{30}\text{O}_{110}$, WS_2 and $\text{GdP}_5\text{W}_{30}\text{O}_{110}@\text{WS}_2$ aqueous solutions ($100 \mu\text{g mL}^{-1}$).

to-obtain heterostructure $\text{GdP}_5\text{W}_{30}\text{O}_{110}@\text{WS}_2$ NCs were synthesized according to the previously reported strategies by a facile amidation reaction activated by 1-(3-dimethylaminopropyl)-3-ethylcarbodiimide (EDC)/N-hydroxysuccinimide (NHS) (Scheme 1A).²⁷ As visualized by the transmission electron microscopy (TEM) image and the average hydrodynamic diameter recorded by dynamic light scattering (DLS) measurement, the as-synthesized $\text{GdP}_5\text{W}_{30}\text{O}_{110}@\text{WS}_2$ NCs showed a uniform and well-dispersed nanostructure and the size of $\text{GdP}_5\text{W}_{30}\text{O}_{110}@\text{WS}_2$ NCs was approximately 60 nm (Fig. 1A and B). Additionally, as presented in Fig. 1C, the changes of zeta potential for the samples could verify the successful surface loading of $\text{GdP}_5\text{W}_{30}\text{O}_{110}$ nanoclusters onto WS_2 nanosheets.²⁷ Furthermore, the Fourier transform infrared (FTIR) spectra and Raman spectra of the different components also affirmed that the as-prepared $\text{GdP}_5\text{W}_{30}\text{O}_{110}@\text{WS}_2$ NCs had specific absorption peaks corresponding to $\text{GdP}_5\text{W}_{30}\text{O}_{110}$ nanoclusters and WS_2 nanosheets (Fig. 1D and E), which is consistent with previously reported work. The strong characteristic peaks at 1164, 1170, 917 and 780 cm^{-1} in $\text{GdP}_5\text{W}_{30}\text{O}_{110}$ nanoclusters are assigned to the stretching vibration of the P–O band, W–O asymmetric vibration and W–O–W asymmetric vibration, respectively. In addition, the chemical composition of $\text{GdP}_5\text{W}_{30}\text{O}_{110}@\text{WS}_2$ NCs was further verified by UV-vis absorption spectra, indicating the successful fabrication (Fig. 1F). Taken together, the heterojunction $\text{GdP}_5\text{W}_{30}\text{O}_{110}@\text{WS}_2$ NCs were successfully fabricated as designed and have the potential for subsequent application in sensitive biomolecule detection.

Peroxidase-like catalytic activity of $\text{GdP}_5\text{W}_{30}\text{O}_{110}@\text{WS}_2$

Peroxidases are a class of enzymes that can catalyze the production of reactive oxygen species (ROS) by applying peroxides (e.g.,

H_2O_2) as substrates, and have been widely used in biological catalysis, biosensing, disease treatment and regulating physiological activities.^{28,29} Until now, a large number of nanomaterials have been shown to possess intrinsic POD-like catalytic activity, the most representative one of which is metal-based nanomaterials with mixed redox states. Inspired by the recent advances, the heterojunction $\text{GdP}_5\text{W}_{30}\text{O}_{110}@\text{WS}_2$ NCs with mixed redox states thus exhibit great potential to exert considerable peroxidase-like catalytic activity. We next investigated the POD-like catalytic activity of $\text{GdP}_5\text{W}_{30}\text{O}_{110}@\text{WS}_2$ NCs in the presence of H_2O_2 through the oxidation of a series of colorimetric substrates (e.g., 3,3',5,5'-tetramethylbenzidine (TMB), 2,2'-azino-bis(3-ethylbenzothiazoline-6-sulfonic acid) (ABTS), and *o*-phenylenediamine (OPD)). As shown in Fig. 2A, due to the intrinsic peroxidase-like catalytic activity of $\text{GdP}_5\text{W}_{30}\text{O}_{110}@\text{WS}_2$ NCs, H_2O_2 could be catalyzed into hydroxyl radicals ($\cdot\text{OH}$) and the reaction solution turned into the corresponding color of the oxidized colorimetric substrates (blue for oxTMB, green for oxABTS, yellow for oxOPD). As indicated in Fig. 2B, no significant characteristic absorbance and color change of TMB alone or TMB + $\text{GdP}_5\text{W}_{30}\text{O}_{110}@\text{WS}_2$ could be found. Meanwhile, the distinct characteristic absorption peaks were observed in the mixture of $\text{GdP}_5\text{W}_{30}\text{O}_{110}@\text{WS}_2$ NCs, H_2O_2 and TMB (green curve), reflecting the efficacious peroxidase-like catalytic activity. Analogously, the maximum absorption peaks of oxABTS and oxOPD in the ABTS/OPD + H_2O_2 + $\text{GdP}_5\text{W}_{30}\text{O}_{110}@\text{WS}_2$ group also implied that $\text{GdP}_5\text{W}_{30}\text{O}_{110}@\text{WS}_2$ NCs exhibited a superior peroxidase-like catalytic performance. Consequently, the prominent peroxidase-like catalytic activity of $\text{GdP}_5\text{W}_{30}\text{O}_{110}@\text{WS}_2$ NCs ensures their further controllable utilization for further application.

Similar to natural enzymes, the catalytic activity of nanzymes is also largely influenced by catalytic conditions, such as concentration, pH and temperature.³⁰ In order to enable



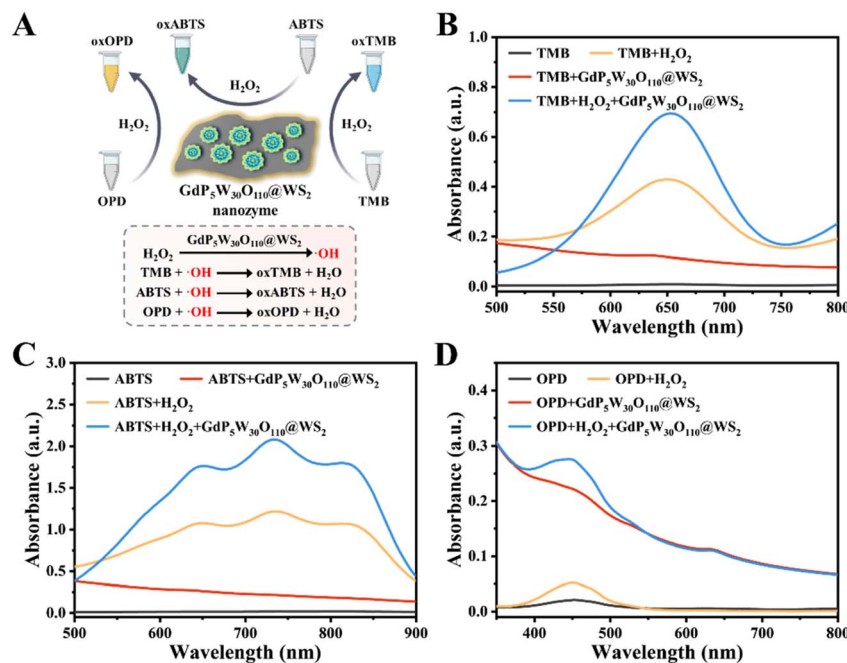


Fig. 2 (A) Schematic illustration of the mechanism for the peroxidase-like activity evaluation of $\text{GdP}_5\text{W}_{30}\text{O}_{110}\text{@WS}_2$ applying TMB, OPD and ABTS as substrates. UV-vis-NIR adsorption spectra of the catalyzed oxidation of (B) TMB, (C) ABTS and (D) OPD after 15 min of incubation with PBS, $\text{GdP}_5\text{W}_{30}\text{O}_{110}\text{@WS}_2$, H_2O_2 and $\text{H}_2\text{O}_2 + \text{GdP}_5\text{W}_{30}\text{O}_{110}\text{@WS}_2$ at pH 4.0.

$\text{GdP}_5\text{W}_{30}\text{O}_{110}\text{@WS}_2$ to realize a maximal catalytic performance, we subsequently explored the optimal catalytic conditions in the classical TMB colorimetric system. As indicated in Fig. 3A and E, along with the increasing concentration of $\text{GdP}_5\text{W}_{30}\text{O}_{110}\text{@WS}_2$, the characteristic absorbance of oxTMB at 652 nm gradually increased, which is mainly attributed to the concentration-dependent peroxidase-like catalytic performance of $\text{GdP}_5\text{W}_{30}\text{O}_{110}\text{@WS}_2$. Meanwhile, $\text{GdP}_5\text{W}_{30}\text{O}_{110}\text{@WS}_2$ exhibited a stable peroxidase-like catalytic activity under acidic experimental conditions (pH at 3.0) and higher temperature

than most natural enzymes (Fig. 3B, C, F and G). Besides, as shown in Fig. 3D and H, maximum catalytic activity was reached with 0.5 mM TMB.

Biomolecule detection by $\text{GdP}_5\text{W}_{30}\text{O}_{110}\text{@WS}_2$

Inspired by the outstanding peroxidase-like catalytic activity of $\text{GdP}_5\text{W}_{30}\text{O}_{110}\text{@WS}_2$, a $\text{GdP}_5\text{W}_{30}\text{O}_{110}\text{@WS}_2$ -based analytical platform was established for biomolecule detection, including H_2O_2 , GSH and glucose detection.

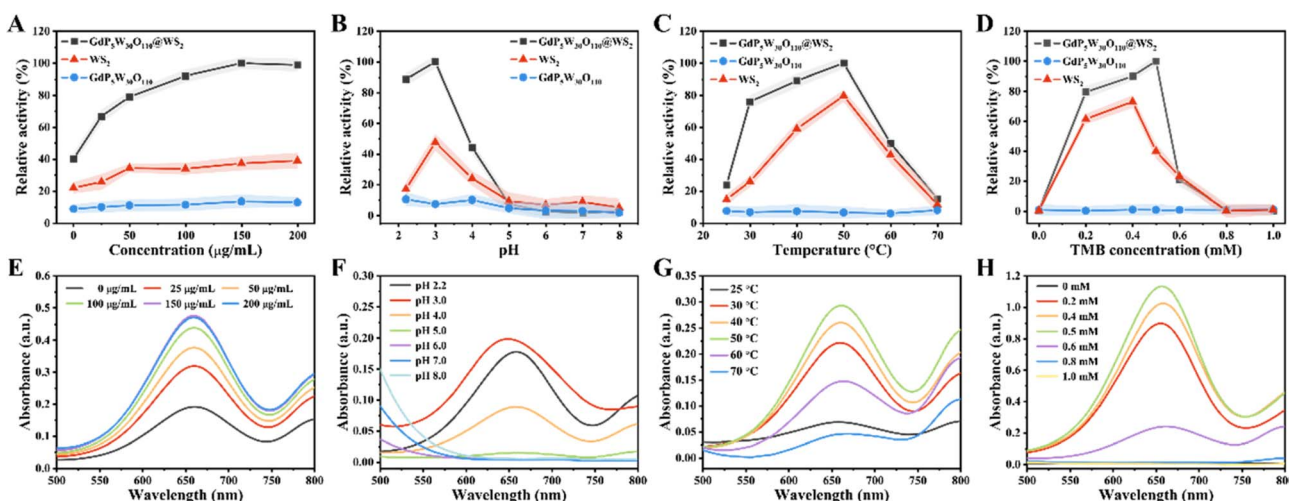


Fig. 3 The optimization of (A) concentration, (B) pH, (C) temperature and (D) TMB concentration for the peroxidase-like activity of $\text{GdP}_5\text{W}_{30}\text{O}_{110}\text{@WS}_2$, $\text{GdP}_5\text{W}_{30}\text{O}_{110}$ and WS_2 calculated from the corresponding absorbance values (E–H). The maximum point in every curve was set to 100%. Error bars represent the standard error derived from three independent measurements.

During the peroxidase-like catalytic process of $\text{GdP}_5\text{W}_{30}\text{O}_{110}@\text{WS}_2$, the absorbance intensity of oxidized substrates could vary according to the experimental conditions, thereby offering reliable evidence for quantifying biomolecules related to H_2O_2 . In detail, $\cdot\text{OH}$ was generated under the POD-like catalytic action of $\text{GdP}_5\text{W}_{30}\text{O}_{110}@\text{WS}_2$ in the presence of H_2O_2 . Subsequently, the formed $\cdot\text{OH}$ would catalyze the oxidation of TMB into oxTMB, which can be easily quantified by monitoring the characteristic absorbance intensity at 652 nm. Conceivably, a higher level of H_2O_2 would lead to higher absorbance intensity (Fig. 4A). For H_2O_2 detection, the characteristic absorbance intensity at 652 nm gradually increased with the increasing addition of H_2O_2 on a low concentration scale. As demonstrated in Fig. 4B and C, H_2O_2 concentration was linearly positively related to the absorbance intensity within the range from 0 to 50 μM .

As one of the most representative endogenous antioxidants in cells, GSH plays a vital part in modulating the balance

between free radicals and the antioxidant defense system.^{31–34} The disorders of GSH homeostasis are closely associated with such diseases as cancer, aging, neurodegenerative diseases and inflammations.³³ Therefore, investigations on convenient and rational methods for GSH detection have aroused widespread concern in biochemical analysis and clinical diagnosis. As a radical scavenger, GSH can quench $\cdot\text{OH}$ released by the POD-like catalytic reaction of $\text{GdP}_5\text{W}_{30}\text{O}_{110}@\text{WS}_2$ with H_2O_2 , giving rise to inhibition of the TMB oxidation process. As shown in Fig. 4A, the generation of $\cdot\text{OH}$ from H_2O_2 catalyzed by $\text{GdP}_5\text{W}_{30}\text{O}_{110}@\text{WS}_2$ could gradually oxidize the substrate TMB into oxTMB. After the introduction of GSH, the released $\cdot\text{OH}$ was depleted and weaker absorbance intensity at 652 nm could be detected. According to the considerable scavenging effect of GSH on $\cdot\text{OH}$, a reliable analytical platform was then constructed for GSH detection. As shown in Fig. 4D, with the increasing concentration of GSH, the absorbance signal at 652 nm responded with a descending trend. Meanwhile, there was

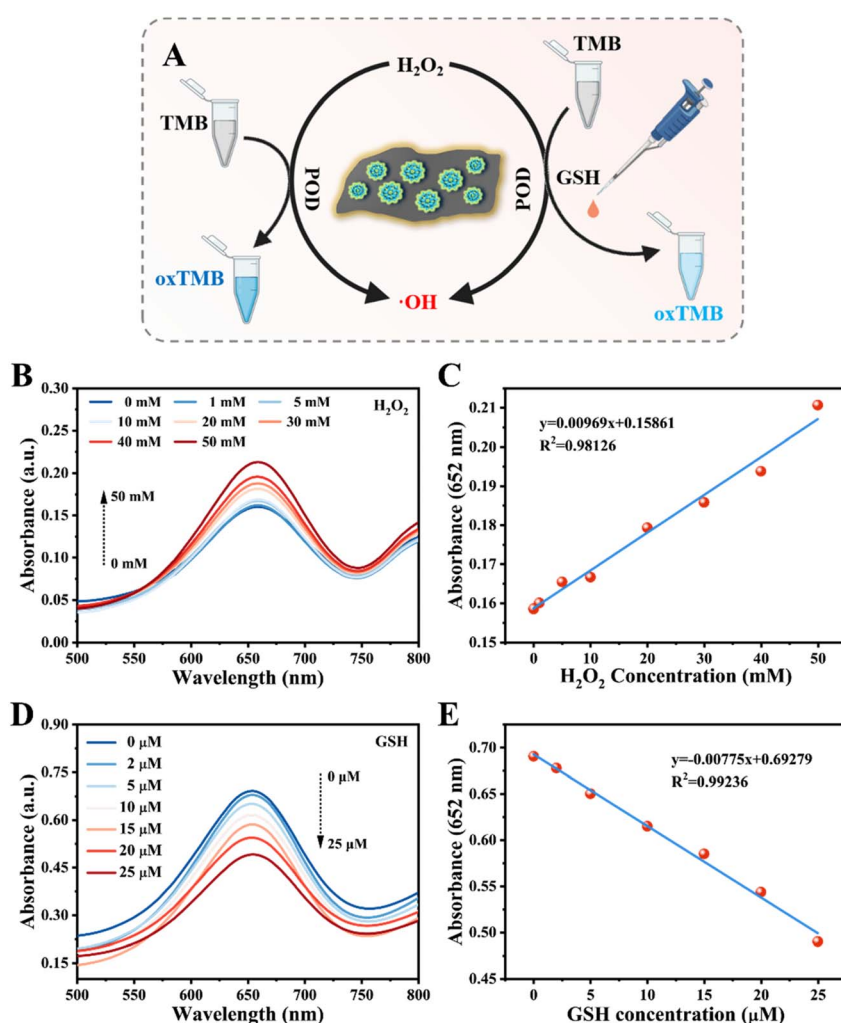


Fig. 4 $\text{GdP}_5\text{W}_{30}\text{O}_{110}@\text{WS}_2$ nanoclusters-based sensing platform for H_2O_2 and GSH detection. (A) Mechanism description of $\text{GdP}_5\text{W}_{30}\text{O}_{110}@\text{WS}_2$ nanozymes with peroxidase-like activity for H_2O_2 and GSH detection. (B) UV-vis-NIR adsorption spectra of $\text{GdP}_5\text{W}_{30}\text{O}_{110}@\text{WS}_2$ ($100 \mu\text{g mL}^{-1}$) incubated with TMB (0.5 mM) in the presence of different concentration of H_2O_2 at pH 4.0. (C) The linear calibration plot for H_2O_2 detection. (D) UV-vis-NIR adsorption spectra of $\text{GdP}_5\text{W}_{30}\text{O}_{110}@\text{WS}_2$ ($100 \mu\text{g mL}^{-1}$) incubated with TMB (0.5 mM) and H_2O_2 (50 mM) in the presence of different concentrations of GSH at pH 4.0. (E) The linear calibration plot for GSH detection.



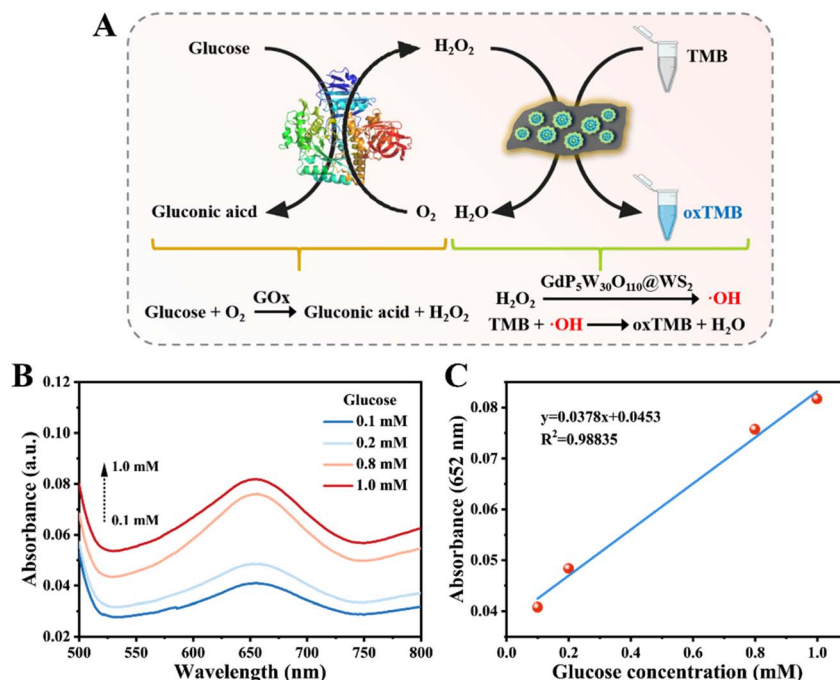


Fig. 5 $\text{GdP}_5\text{W}_{30}\text{O}_{110}\text{@WS}_2$ nanoclusters-based sensing platform for glucose detection. (A) Mechanism description of $\text{GdP}_5\text{W}_{30}\text{O}_{110}\text{@WS}_2$ nanozymes with peroxidase-like activity for glucose detection. (B) UV-vis-NIR adsorption spectra of $\text{GdP}_5\text{W}_{30}\text{O}_{110}\text{@WS}_2$ ($100 \mu\text{g mL}^{-1}$) incubated with TMB (0.5 mM) and GOx (1 mg mL^{-1}) in the presence of different concentrations of glucose at pH 4.0. (C) The linear calibration plot for glucose detection.

a satisfactory linear correlation between the absorbance intensity and GSH concentration ranging from 0 to $25 \mu\text{M}$.

Glucose is the impetus of cell metabolism and is a universally available energy source for ATP production.³³ In the presence of glucose oxidase (GOx), glucose can be effectively translated into gluconic acid and H₂O₂. In this regard, assisted by GOx-triggered oxidation, the generated H₂O₂ can act as a mediate substrate for glucose detection. After linear fitting, it was found that the $\text{GdP}_5\text{W}_{30}\text{O}_{110}\text{@WS}_2$ -based analytical platform was able to detect glucose in a range from 0.1 to 1 mM (Fig. 5).

These content results indicated the potential application value of the proposed $\text{GdP}_5\text{W}_{30}\text{O}_{110}\text{@WS}_2$ -based analytical platform for biomolecule detection.

Conclusion

In conclusion, heterojunction $\text{GdP}_5\text{W}_{30}\text{O}_{110}\text{@WS}_2$ possessing intrinsic POD-like activity was prepared by a simple approach. As proved by our primary experiments, the proposed heterojunction $\text{GdP}_5\text{W}_{30}\text{O}_{110}\text{@WS}_2$ can generally oxidize several colorimetric substrates such as TMB, ABTS, and OPD in the presence of H₂O₂. Meanwhile, assisted by the excellent POD-like catalytic activity, the fabricated $\text{GdP}_5\text{W}_{30}\text{O}_{110}\text{@WS}_2$ was introduced as a probe for the sensitive detection of H₂O₂, GSH and glucose. All of the above favorable results highlighted that this work provided more possibilities for the construction of multifunctional polyoxometalate-based nanomaterials for biosensing, greatly expanding the potential value of other nanozyme-based biosensors.

Author contributions

Guobo Du and Mingzhu Lv contributed equally to this work. Yuan Yong and Guobo Du conceived and supervised this project. Mingzhu Lv, Chenghui Liu, Jiajie Liu, Zhu Yang, Huan Wang and Qiqi Xu performed the experiments and analysed the data. Yuan Yong, Guobo Du and Mingzhu Lv revised the paper. All authors have reviewed and approved the final version of this manuscript.

Conflicts of interest

The authors declare no conflict of interest.

Acknowledgements

This work was financially supported by the National Natural Science Foundation of China (31901005 and 52273304), the Natural Science Foundation of Sichuan Province (2022NSFSC0796), the Southwest Minzu University Talent Supporting Funds (RQD2021008), Scientific research and development funds of Affiliated Hospital of North Sichuan Medical College (2021ZD013), Nanchong City-School Cooperative Scientific Research Funds (20SXZRKX0006), Young Elite Scientists Sponsorship Program by CAST (YESS) (2022-2024QNRC001), the Open Project of Central Nervous System Drug Key Laboratory of Sichuan Province (230011-01SZ) and the Fundamental Research Funds for the Central Universities, Southwest Minzu University (2021NYYXS30).



References

1 G. Maduraiveeran, M. Sasidharan and V. Ganesan, Electrochemical sensor and biosensor platforms based on advanced nanomaterials for biological and biomedical applications, *Biosens. Bioelectron.*, 2018, **103**, 113–129.

2 S. K. Krishnan, E. Singh, P. Singh, M. Meyyappan and H. S. Nalwa, A review on graphene-based nanocomposites for electrochemical and fluorescent biosensors, *RSC Adv.*, 2019, **9**, 8778–8881.

3 W. Q. Xu, L. Jiao, Y. Wu, L. Y. Hu, W. L. Gu and C. Z. Zhu, Metal-Organic Frameworks Enhance Biomimetic Cascade Catalysis for Biosensing, *Adv. Mater.*, 2021, **33**, 2005172.

4 C. Song, W. Ding, W. W. Zhao, H. B. Liu, J. Wang, Y. W. Yao and C. Yao, High peroxidase-like activity realized by facile synthesis of FeS_2 nanoparticles for sensitive colorimetric detection of H_2O_2 and glutathione, *Biosens. Bioelectron.*, 2020, **151**, 111983.

5 B. F. Wang, Y. Y. Luo, L. Gao, B. Liu and G. T. Duan, High-performance field-effect transistor glucose biosensors based on bimetallic Ni/Cu metal-organic frameworks, *Biosens. Bioelectron.*, 2021, **171**, 112736.

6 Z. H. Zhao, Y. J. Huang, W. R. Liu, F. G. Ye and S. L. Zhao, Immobilized Glucose Oxidase on Boronic Acid-Functionalized Hierarchically Porous MOF as an Integrated Nanozyme for One-Step Glucose Detection, *ACS Sustainable Chem. Eng.*, 2020, **8**, 4481–4488.

7 Y. Chong, Q. Liu and C. C. Ge, Advances in oxidase-mimicking nanozymes: Classification, activity regulation and biomedical applications, *Nano Today*, 2021, **37**, 101076.

8 Z. R. Wang, R. F. Zhang, X. Y. Yan and K. L. Fan, Structure and activity of nanozymes: Inspirations for de novo design of nanozymes, *Mater. Today*, 2020, **41**, 81–119.

9 N. F. Zhu, C. B. Liu, R. Liu, X. H. Niu, D. H. Xiong, K. Wang, D. Q. Yin and Z. Zhang, Biomimic Nanozymes with Tunable Peroxidase-like Activity Based on the Confinement Effect of Metal-Organic Frameworks (MOFs) for Biosensing, *Anal. Chem.*, 2022, **94**, 4821–4830.

10 L. Huang, Y. Zhou, Y. X. Zhu, H. Y. Su, S. Z. Yang, L. Feng, L. Zhao, S. R. Liu and K. Qian, Dual-modal nanoplatform integrated with smartphone for hierarchical diabetic detection, *Biosens. Bioelectron.*, 2022, **210**, 114254.

11 L. Z. Gao, J. Zhuang, L. Nie, J. B. Zhang, Y. Zhang, N. Gu, T. H. Wang, J. Feng, D. L. Yang, S. Perrett and X. Y. Yan, Intrinsic peroxidase-like activity of ferromagnetic nanoparticles, *Nat. Nanotechnol.*, 2007, **2**, 577–583.

12 M. Wang, M. Y. Chang, Q. Chen, D. M. Wang, C. X. Li, Z. Y. Hou, J. Lin, D. Y. Jin and B. G. Xing, Au₂Pt-PEG-Ce₆ nanoformulation with dual nanozyme activities for synergistic chemodynamic therapy/phototherapy, *Biomaterials*, 2020, **252**, 120093.

13 W. C. Hu, M. R. Younis, Y. Zhou, C. Wang and X. H. Xia, In Situ Fabrication of Ultrasmall Gold Nanoparticles/2D MOFs Hybrid as Nanozyme for Antibacterial Therapy, *Small*, 2020, **16**, 2000553.

14 X. Q. Meng, D. D. Li, L. Chen, H. L. He, Q. Wang, C. Y. Hong, J. Y. He, X. F. Gao, Y. L. Yang, B. Jiang, G. H. Nie, X. Y. Yan, L. Z. Gao and K. L. Fan, High-Performance Self-Cascade Pyrite Nanozymes for Apoptosis-Ferroptosis Synergistic Tumor Therapy, *ACS Nano*, 2021, **15**, 5735–5751.

15 F. Wei, X. Y. Cui, Z. Wang, C. C. Dong, J. D. Li and X. J. Han, Recoverable peroxidase-like Fe₃O₄@MoS₂-Ag nanozyme with enhanced antibacterial ability, *Chem. Eng. J.*, 2021, **408**, 127240.

16 Z. W. Liu, X. Y. Zhao, B. R. Yu, N. N. Zhao, C. Zhang and F. J. Xu, Rough Carbon-Iron Oxide Nanohybrids for Near-Infrared-II Light-Responsive Synergistic Antibacterial Therapy, *ACS Nano*, 2021, **15**, 7482–7490.

17 M. Y. Chang, Z. Y. Hou, M. Wang, C. Z. Yang, R. F. Wang, F. Li, D. L. Liu, T. L. Peng, C. X. Li and J. Lin, Single-Atom Pd Nanozyme for Ferroptosis-Boosted Mild-Temperature Photothermal Therapy, *Angew. Chem., Int. Ed.*, 2021, **60**, 12971–12979.

18 J. Kong, J. Zheng, Z. M. Li, J. B. Huang, F. H. Cao, Q. Zeng and F. Li, One-pot synthesis of AuAgPd trimetallic nanoparticles with peroxidase-like activity for colorimetric assays, *Anal. Bioanal. Chem.*, 2021, **413**, 5383–5393.

19 B. J. Ma, S. Wang, F. Liu, S. Zhang, J. Z. Duan, Z. Li, Y. Kong, Y. H. Sang, H. Liu, W. B. Bu and L. L. Li, Self-Assembled Copper Amino Acid Nanoparticles for in Situ Glutathione “AND” H_2O_2 Sequentially Triggered Chemodynamic Therapy, *J. Am. Chem. Soc.*, 2019, **141**, 849–857.

20 Z. L. Dong, L. Z. Feng, Y. Chao, Y. Hao, M. C. Chen, F. Gong, X. Han, R. Zhang, L. Cheng and Z. Liu, Amplification of Tumor Oxidative Stresses with Liposomal Fenton Catalyst and Glutathione Inhibitor for Enhanced Cancer Chemotherapy and Radiotherapy, *Nano Lett.*, 2019, **19**, 805–815.

21 L. W. Wang, B. Li, Z. You, A. Z. Wang, X. Y. Chen, G. J. Song, L. Yang, D. Chen, X. Yu, J. Liu and C. Y. Chen, Heterojunction of Vertically Arrayed MoS₂ Nanosheet/N-Doped Reduced Graphene Oxide Enabling a Nanozyme for Sensitive Biomolecule Monitoring, *Anal. Chem.*, 2021, **93**, 11123–11132.

22 G. T. Wang, T. Wang, Y. Dang, Z. W. Lu, G. H. Su, B. Feng, Y. Zhuo, X. M. Jiang, Q. B. Ye, C. Wu, X. Pu, Y. Zhao, X. Q. Zhao, S. Cai, S. Y. Du, S. S. Jia, Y. Y. Wang, D. Wu, H. B. Rao and M. M. Sun, Insights into the antibacterial mechanism of MoS₂/CoS₂ heterostructure nanozymes with double enzyme-like activities for MRSA-infected wound therapy, *Chem. Eng. J.*, 2023, **461**, 141959.

23 L. W. Wang, Z. W. Yang, G. X. Song, Z. You, X. Y. Zhang, L. Liu, J. Zhang, L. H. Ding, N. Ren, A. Z. Wang, J. Liu, L. Liu and X. Yu, Construction of S-N-C bond for boosting bacteria-killing by synergistic effect of photocatalysis and nanozyme, *Appl. Catal., B*, 2023, **325**, 122345.

24 L. W. Wang, F. N. Gao, A. Z. Wang, X. Y. Chen, H. Li, X. Zhang, H. Zheng, R. Ji, B. Li, X. Yu, J. Liu, Z. J. Gu, F. L. Chen and C. Y. Chen, Defect-Rich Adhesive Molybdenum Disulfide/rGO Vertical Heterostructures with Enhanced Nanozyme Activity for Smart Bacterial Killing Application, *Adv. Mater.*, 2020, **32**, 2005423.



25 S. Cardona-Serra, J. M. Clemente-Juan, E. Coronado, A. Gaita-Arino, A. Camon, M. Evangelisti, F. Luis, M. J. Martinez-Perez and J. Sese, Lanthanoid Single-Ion Magnets Based on Polyoxometalates with a 5-fold Symmetry: The Series $[\text{LnP}_5\text{W}_{30}\text{O}_{110}]^{12-}$ ($\text{Ln}^{3+} = \text{Tb}, \text{Dy}, \text{Ho}, \text{Er}, \text{Tm}, \text{and Yb}$), *J. Am. Chem. Soc.*, 2012, **134**, 14982–14990.

26 Y. Yong, L. J. Zhou, Z. J. Gu, L. Yan, G. Tian, X. P. Zheng, X. D. Liu, X. Zhang, J. X. Shi, W. S. Cong, W. Y. Yin and Y. L. Zhao, WS₂ nanosheet as a new photosensitizer carrier for combined photodynamic and photothermal therapy of cancer cells, *Nanoscale*, 2014, **6**, 10394–10403.

27 L. Y. Zong, H. X. Wu, H. Lin and Y. Chen, A polyoxometalate-functionalized two-dimensional titanium carbide composite MXene for effective cancer theranostics, *Nano Res.*, 2018, **11**, 4149–4168.

28 B. W. Yang, Y. Chen and J. L. Shi, Reactive Oxygen Species (ROS)-Based Nanomedicine, *Chem. Rev.*, 2019, **119**, 4881–4985.

29 M. Y. Chang, M. Wang, M. F. Wang, M. M. Shu, B. B. Ding, C. X. Li, M. L. Pang, S. Z. Cui, Z. Y. Hou and J. Lin, A Multifunctional Cascade Bioreactor Based on Hollow-Structured Cu₂MoS₄ for Synergetic Cancer Chemo-Dynamic Therapy/Starvation Therapy/Phototherapy/Immunotherapy with Remarkably Enhanced Efficacy, *Adv. Mater.*, 2019, **31**, 1905271.

30 Y. Y. Huang, J. S. Ren and X. G. Qu, Nanozymes: Classification, Catalytic Mechanisms, Activity Regulation, and Applications, *Chem. Rev.*, 2019, **119**, 4357–4412.

31 G. X. Yin, T. T. Niu, T. Yu, Y. B. Gan, X. Y. Sun, P. Yin, H. M. Chen, Y. Y. Zhang, H. T. Li and S. Z. Yao, Simultaneous Visualization of Endogenous Homocysteine, Cysteine, Glutathione, and their Transformation through Different Fluorescence Channels, *Angew. Chem., Int. Ed.*, 2019, **58**, 4557–4561.

32 L. S. Lin, J. B. Song, L. Song, K. M. Ke, Y. J. Liu, Z. J. Zhou, Z. Y. Shen, J. Li, Z. Yang, W. Tang, G. Niu, H. H. Yang and X. Y. Chen, Simultaneous Fenton-like Ion Delivery and Glutathione Depletion by MnO₂-Based Nanoagent to Enhance Chemodynamic Therapy, *Angew. Chem., Int. Ed.*, 2018, **57**, 4902–4906.

33 N. Ballatori, S. M. Krance, S. Notenboom, S. J. Shi, K. Tieu and C. L. Hammond, Glutathione dysregulation and the etiology and progression of human diseases, *Biol. Chem.*, 2009, **390**, 191–214.

34 J. S. Huang, Y. C. Li, L. Zhang, J. Wang, Z. G. Xu, Y. J. Kang and P. Xue, A platinum nanourchin-based multi-enzymatic platform to disrupt mitochondrial function assisted by modulating the intracellular H₂O₂ homeostasis, *Biomaterials*, 2022, **286**, 121572.

